Provided for non-commercial research and education use.
Not for reproduction, distribution or commercial use.

This article appeared in a journal published by Elsevier. The attached copy is furnished to the author for internal non-commercial research and education use, including for instruction at the authors institution and sharing with colleagues.

Other uses, including reproduction and distribution, or selling or licensing copies, or posting to personal, institutional or third party websites are prohibited.

In most cases authors are permitted to post their version of the article (e.g. in Word or Tex form) to their personal website or institutional repository. Authors requiring further information regarding Elsevier's archiving and manuscript policies are encouraged to visit:

http://www.elsevier.com/copyright

Author's personal copy

Combustion and Flame 156 (2009) 5–13

Contents lists available at ScienceDirect

Combustion and Flame

www.elsevier.com/locate/combustflame

Effect of particle size on combustion of aluminum particle dust in air

Ying Huang, Grant A. Risha, Vigor Yang *, Richard A. Yetter

Department of Mechanical and Nuclear Engineering, The Pennsylvania State University, University Park, PA 16802, USA

ARTICLE INFO

Article history:
Received 3 March 2007
Received in revised form 14 July 2008
Accepted 17 July 2008
Available online 5 November 2008

Keywords:
Nano-particle
Micron-sized particle
Aluminum combustion
Diffusion-controlled
Kinetically controlled

ABSTRACT

The combustion of aluminum particle dust in a laminar air flow is theoretically studied under fuel-lean conditions. A wide range of particle sizes at nano and micron scales is explored. The flame speed and temperature distribution are obtained by numerically solving the energy equation in the flame zone, with the particle burning rate modeled as a function of particle diameter and ambient temperature. The model allows for investigation into the effects of particle size, equivalence ratio, and chemical kinetics on the burning characteristics and flame structures of aluminum-particle/air mixtures. In addition, the flame behavior with ultra-fine particles in the sub-nanometer range is examined by asymptotically treating particles as large molecules. Calculated flame speeds show reasonable agreement with experimental data. As the particle diameter decreases from the micron to the nano range, the flame speed increases and the combustion transits from a diffusion-controlled to a kinetically controlled mode. For micron-sized and larger particles, the flame speed can be correlated with the particle size according to a d^{-m} relationship, with m being 0.92. For nano-particles, a $d^{-0.52}$ or $d^{-0.13}$ dependence is obtained, depending on whether the $d^{1.0}$- or $d^{0.3}$-law of particle burning time is implemented in the flame model, respectively. No universal law of flame speed exists for the entire range of particle sizes.

© 2008 Published by Elsevier Inc. on behalf of The Combustion Institute.

1. Introduction

Combustion of particle-laden flows is critical to the development of energy-conversion systems using particulates as the primary fuel. Results can provide valuable information to guide the design of particle injection, ignition, flame stabilization, and combustor thermal management. Cassel [1] conducted experimental studies of flame propagation in mixtures containing aluminum dust and air by means of both Bunsen-type and flat-dust-flame burners. Ballal [2] examined the burning behavior of the flat flame in an aluminum–air mixture in a freely falling tube, simulating a microgravity condition. In those two pioneering works, lean-dust mixtures were tested, and the burning velocity was found to increase with the dust concentration. Goroshin et al. [3] later measured the flame speed of aluminum dust in various oxidizer environments in a vertical Pyrex tube over a wide range of dust concentrations of 0.13–0.60 kg/m^3 ($0.42 < \phi < 2.0$ for dust–air mixtures). Goroshin et al. [4] also developed an experimental apparatus capable of producing Bunsen-type premixed dust flames of aluminum mixtures. The dust mass concentration, β, covered a range of 0.25–0.60 kg/m^3, corresponding to a range of equivalence ratios, ϕ, of 0.81–1.9. Both experiments indicated a weak dependence of the burning velocity on the dust concentration for fuel-rich mixtures, a phenomenon that can be attributed to the insensitivity of the particle burning rate to the flame temperature in the diffusive regime. Shoshin and Dreizin [5] developed a lifted-flame aerosol burner for measuring laminar flame speeds of fuel-rich aluminum–air aerosols with particle mass concentrations of 0.4–1.4 kg/m^3 ($1.3 < \phi < 4.5$). A decrease in the flame speed with a very high mass concentration was observed. Combustion of dual-fuel particle-laden flows was examined by Boichuk et al. [6] and Goroshin et al. [7] for micron-sized aluminum–boron and aluminum–manganese dust mixtures, respectively.

Risha et al. [8] recently examined the flame characteristics of bimodal nano/micron-sized aluminum particle dust in air using a Bunsen-burner type of apparatus, similar to the experiment of Goroshin et al. [4]. The particle compositions ranged from 100% micron-sized particles (5–8 μm) to 30% nano-particles (100 nm) by mass in the fuel formulation. The overall fuel concentration varied from 0.26 to 0.45 kg/m^3 ($0.81 \leqslant \phi \leqslant 1.62$). Results indicated that the flame thickness of a bimodal nano/micron-sized particle/air mixture was much wider than its counterpart for micro-sized particles. An increase in the percentage of nano-particles within the mixture enhanced the flame speed. Detailed flame structures of bimodal mixtures and mechanisms responsible for the increased burning velocities by addition of nano-particles were theoretically investigated in Ref. [9].

In spite of the extensive use of aluminum particles to improve the energy density and combustion stability characteristics of propulsion systems [10–12], most existing studies have dealt with micron-sized particles [13–16]. Information about particle

* Corresponding author. Fax: +1 814 865 3389.
E-mail address: vigor@psu.edu (V. Yang).

0010-2180/$ – see front matter © 2008 Published by Elsevier Inc. on behalf of The Combustion Institute.
doi:10.1016/j.combustflame.2008.07.018

Author's personal copy

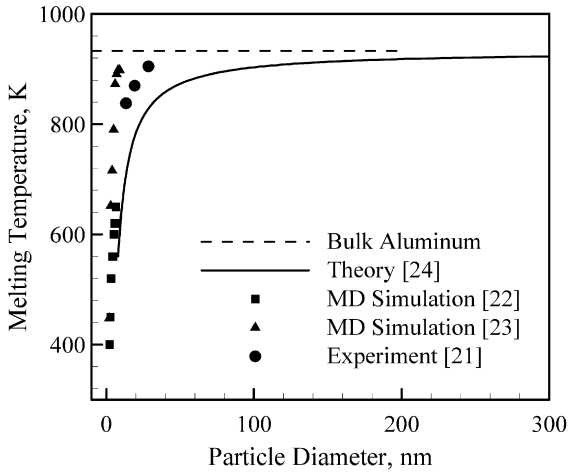

Fig. 1. Aluminum melting temperature as a function of particle diameter.

burning behavior at nano scales remains limited [17–20]. As a consequence of their high specific surface area and ensuing high reactivities, nano-metallic particles exhibit many features distinct from micron-sized or larger particles, including lower ignition temperatures and faster burning rates. The surface-to-volume ratio for a very fine particle may reach a level such that the surface energy may qualitatively change the "bulk" properties of the material, including the melting temperature, enthalpy of fusion, and boiling temperature. Eckert et al. [21] experimentally studied the melting behavior of nano-crystalline aluminum powders using differential scanning calorimetry. The particles were synthesized by mechanical attrition under different atmospheres with sizes ranging from 13 to 40 nm. Alavi and Thompson [22] and Puri and Yang [23] conducted molecular-dynamics (MD) studies of the melting of aluminum particles in the ranges of 1.0–3.4 nm and 2–9 nm, respectively. Analytical models based on classical thermodynamics theories were also developed for the size dependence of the melting point of metal particles [24]. Fig. 1 shows the aluminum melting temperature as a function of particle diameter. The melting temperature decreases gradually with decreasing particle size up to 10 nm. When the particle size is smaller than this critical value, a drastic decrease in the melting temperatures occurs. Molecular-dynamics simulations of [22,23] indicated that the melting temperature of a 1-nm aluminum particle could be as low as 400 K, which is about 500 K lower than the bulk value of 933 K. Particle diameter also plays a significant role in determining the ignition and combustion mechanisms through its influence on the characteristic transport (i.e., diffusion) times relative to the chemical kinetics time. A large particle at high pressure may burn under diffusion-controlled conditions, whereas a small particle at low pressure may burn under kinetically controlled conditions [12, 25–27] (i.e., the diffusion rate of oxidizer is much faster than the reaction rate at the particle surface). Bazyn et al. [28] studied the combustion of 10-μm aluminum particles at an elevated ambient temperature of 2650 K in the pressure range of 3–30 atm. The particle burning time in oxygen was observed to be strongly dependent on pressure, suggesting that surface chemical processes exert a significant influence on the overall combustion behavior of the 10-μm aluminum particles considered in their study.

The preceding studies have provided much useful information about the combustion of aluminum particles. The current understanding, however, is far from complete, especially in terms of the effects of particle size on dust-flame characteristics. In our previous work [9], the flame properties of aluminum particle-laden flows with a bimodal distribution of particle size were studied experimentally and analytically. The present study provides a further investigation of the combustion of mono-dispersed aluminum particle dust in air. A wide range of particle sizes is considered, with special attention given to nano-particles, whose combustion behavior is kinetically controlled, as opposed to the diffusion-controlled combustion of micron-sized particles. In addition, the flame behavior of ultra-fine particles in the sub-nanometer range is examined in an asymptotic limit by treating particles as large molecules. The influence of chemical kinetics is also analyzed.

2. Theoretical framework

A theoretical model is established to describe steady, one-dimensional, planar flame propagation in a mono-dispersed aluminum particle dust with air. Both diffusion- and kinetically controlled combustion of micron- and nano-sized particles is considered. The present analysis extends the analytical model described in Ref. [9] for treating the combustion of bimodal aluminum particles to include the coupling effects between the particle burning time, ambient flow conditions, and two-phase transport, which usually prevail in flames with nano-sized particles. The major approximations and assumptions adopted in the analysis are: (1) the dust cloud consists of uniformly distributed aluminum particles with air; (2) gravitational effects and heat transfer by radiation are neglected; (3) collisions and interactions between burning particles are neglected; (4) the particle velocity is approximately equal to the gas velocity, considering that the Stokes number is small; and (5) the particle temperature is approximately equal to the surrounding gas temperature, considering that the particle thermal relaxation time is much smaller than the flow residence time in the flame zone.

The governing equations for mass and energy conservation can be written respectively as follows:

$$\rho v = \rho_u S_L, \tag{1}$$

$$\rho v \frac{d}{dx}(CT) = \frac{d}{dx}\left(\lambda \frac{dT}{dx}\right) + w_F \cdot Q, \tag{2}$$

where S_L is the flame speed, w_F the mass consumption rate of particles, Q the heat of reaction per unit mass of fuel, and ρ, v, T the mixture density, velocity, and temperature, respectively. The subscript u denotes the value related to the unburned mixture. The heat capacity of the mixture, C, is defined as $C = C_p + 4\pi r_p^3 C_s \rho_p n_p / 3\rho_g$, where C_p and C_s are the values for the gas and particle, respectively, ρ_p the material density of aluminum, ρ_g the gas density, and n_p the number density of particles (i.e., the number of particles per unit volume).

In the current analysis, we are primarily concerned with fuel-lean mixtures, because of their broad applications. The flame is assumed to consist of a preheat zone and a heat-release zone. In the preheat zone, chemical reactions are neglected, and the flow is heated by conduction from the flame zone. Particles are ignited and then totally consumed in the heat-release zone. For a fuel-lean mixture, the particle-burning time is assumed to be equal to that of a single isolated particle, τ_b, which is a function of the particle diameter, d_p, ambient temperature, T, and local oxidizer concentration, X. As will be shown later, the temperature dependence of burning time is much stronger for nano-particles than for micron-sized particles. Considering that the particle thermal relaxation time is much smaller than the flow residence time in the flame zone, the particle mass consumption can be modeled as $w_F = B_u/\tau_b$, where $B_u = n_p \cdot M_{p0}$ is the initial mass concentration of particulate fuel, with M_p being the mass of a single particle. The heat source term in Eq. (2) can be written as

$$w_F Q = -B_u Q/\tau_b. \tag{3}$$

Author's personal copy

Substituting Eqs. (1) and (3) into Eq. (2), the energy equation for the mixture in the heat-release zone becomes

$$\rho_u S_L \frac{d}{dx}(CT) = \frac{d}{dx}\left(\lambda \frac{dT}{dx}\right) - \frac{B_u Q}{\tau_b}. \tag{4}$$

To monitor the progress of particle burning and to close the formulation, the following equation for the rate of particle mass consumption is derived:

$$\frac{dM_p}{dt} = -\frac{M_{p0}}{\tau_b}. \tag{5}$$

Multiplying the above equation by ρv and rearranging the result, we obtain

$$\frac{d(d_p^3)}{dx} = -\frac{T_u}{T}\frac{d_{p0}^3}{S_L \cdot \tau_b}. \tag{6}$$

To facilitate analysis, the temperature and spatial coordinate are normalized as follows:

$$\theta = \frac{T}{T_u}, \qquad \eta = \frac{d_p}{d_{p0}}, \qquad y = \frac{x'}{S_L \tau_0}, \tag{7}$$

where x' is a density-weighted coordinate, $x' = \int_0^x (\rho/\rho_u)\,dx$, and τ_0 is a reference time scale defined as the burning time of a particle based on its initial size. The location $y = 0$ is defined as the ignition point of particles. To further simplify the model, the thermal conductivity of the mixture, λ, is assumed to be linearly proportional to temperature T, $\lambda = \lambda_u \cdot T/T_u$. Substituting those normalized parameters defined in Eq. (7) into Eqs. (4) and (6), we obtain the following non-dimensional equations for the two different regimes in the flame zone along with their respective boundary conditions.

Preheat zone:

$$\begin{aligned} &\frac{d^2\theta}{dy^2} - \kappa^2 \frac{d\theta}{dy} = 0; \\ &y \to -\infty: \quad \theta = 1. \end{aligned} \tag{8}$$

Heat-release zone:

$$\frac{d^2\theta}{dy^2} - \kappa^2 \frac{d\theta}{dy} = -\mu\kappa^2(\theta_{si} - 1)\theta \frac{\tau_0}{\tau_b};$$

$$\begin{cases} y = 0: \quad \theta = \theta_{si}, \quad \frac{d\theta}{dy}\big|_{0+} = \frac{d\theta}{dy}\big|_{0-}, \\ y \to \infty: \quad \frac{d\theta}{dy} = 0. \end{cases} \tag{9}$$

$$\frac{d\eta}{dy} = -\frac{1}{3\eta^2}\frac{\tau_0}{\tau_b};$$

$$\begin{cases} y = 0: \quad \eta = 1, \\ y \to \infty: \quad \eta = 0. \end{cases} \tag{10}$$

Here θ_{si} is the non-dimensional ignition temperature, and $\kappa = S_L \cdot \sqrt{\tau_0/\alpha}$ the non-dimensional flame speed, with $\alpha = \lambda_u/(C \cdot \rho_u)$ being the thermal diffusivity of the mixture. The non-dimensional heat-release rate, μ, is written as

$$\mu = \frac{-B_u \cdot Q}{\rho_u C \cdot (T_{\text{ign}} - T_u)}. \tag{11}$$

As will be shown later, the particle-burning rate depends on the ambient flow temperature and oxidizing species, a phenomenon especially true for nano-sized particles. An analytical solution to Eqs. (8)–(10) is usually not available and must be obtained using numerical techniques. In the present study, the temperature and heat-flux distribution are first determined analytically in the preheat zone in terms of the flame speed. Equations (9) and (10) are then solved as a two-point boundary-value problem for the heat-release zone, with the flame speed treated as the eigenvalue.

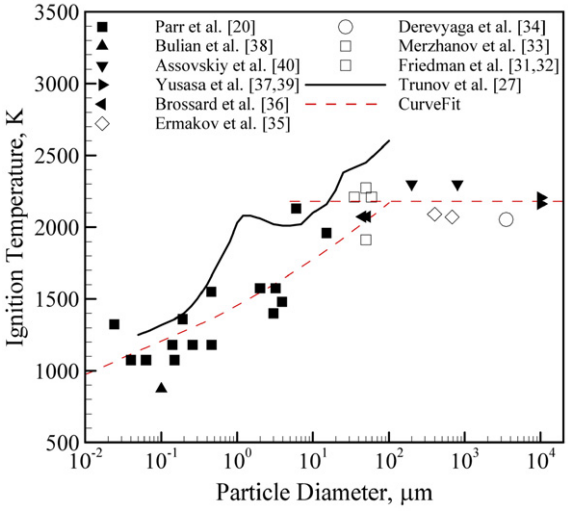

Fig. 2. Ignition temperature of aluminum particle as a function of particle diameter in oxygen-containing environments.

The shooting technique along with the Newton–Raphson iteration method is employed for root finding. The numerical integration of Eqs. (9) and (10) is achieved by means of the Rosenbrock method [29,30].

3. Ignition temperature and particle burning rate

The particle ignition temperature and burning rate must be specified as input parameters in the present analysis. Fig. 2 shows the experimentally observed aluminum-particle ignition temperature as a function of particle size in oxygen-containing environments [31–40]. For particles with diameters greater than 100 μm, the majority of experimental studies have shown that ignition takes place at a temperature near the melting point of aluminum oxide (i.e., 2350 K). Since each aluminum particle is covered by an impervious oxide shell, it was argued that the particle does not ignite until the oxide shell melts or breaks up near its melting temperature under the effect of aluminum thermal expansion. For particles with diameters of 1–100 μm, however, ignition could be achieved over a wide range of temperatures from 1300 to 2300 K. For nano-sized particles, ignition has been reported to occur at temperatures as low as 900 K [20,38]. Such a low ignition temperature may be attributed to the aluminum oxidation and polymorphic phase transformation of the alumina shell [27,41], or to the rupture of the oxide layer due to thermal expansion [42]. In the present study, results from curve-fitting of the experimental data, as shown by the dashed line in Fig. 2, are used for the particle ignition temperature.

Numerous experimental studies have been conducted to determine the particle burning time for micron-sized and larger particles. The size dependence of the burning time usually does not follow the classical d^2-law, but a more general d^n-model, with n ranging from 1.5 to 2.0. It was suggested that the oxide lobe accumulated on the particle surface during the burning process leads to a reduced exponent. In Ref. [43], almost 400 data points for single-particle burning times in various oxidizer environments were collected from more than ten different sources. The following particle burning-time correlation was established:

$$\tau_b = C_1 d^{1.8} / \left(T_0^{0.2} p^{0.1} X_{\text{eff}}\right), \tag{12}$$

where X_{eff} is the effective oxidizer mole fraction, $X_{\text{eff}} = C_{O_2} + 0.6C_{H_2O} + 0.22C_{CO_2}$, p the pressure in atmosphere, T_0 the initial temperature in Kelvin, d the particle diameter in μm, and C_1 a constant ($= 7.35 \times 10^{-6}$). The burning time τ_b is measured in seconds.

Author's personal copy

The $d^{1.8}$-law is employed herein for micron-sized and larger particles. It is worth noting that micron-sized particles usually burn under diffusion-controlled conditions. Recent studies of Bazyn et al. [28,44] and Huang et al. [9], however, indicate that the transition from a diffusion-controlled to a kinetically controlled burning mode may take place at particle diameters on the order of several micrometers.

For nano-sized or small micron-sized particles, which burn under kinetically controlled conditions, it is theoretically expected that a $d^{1.0}$-model with dominant surface reactions may be more suitable for modeling the particle burning time [25]. Parr et al. [20] examined the combustion characteristics of aluminum particles in the diameter range of 24 nm to 30 μm using a hydrogen–oxygen–argon burner. Particles ignited and burned in the post-combustion gases of the burner flame. The flame temperature was controlled between 900 and 2400 K by varying the amount of argon. The experimental setup allowed measurements of the burning times of individual particles, or the ensemble burning time under low loading density if the particles were very small. The effects of particle agglomeration were not detected. It was observed that the burning times of nano-particles are strongly dependent on the burner flame temperature, in contrast to the burning times for micron-sized particles, which are only weakly dependent on the environmental gas temperature, as suggested by Eq. (12). This difference results from the absence of an enveloped flame in the case of nano-particles, whereas one would exist for micron-sized particles. For the particles considered in [20], a $d^{0.3}$-law is established below instead of a $d^{1.0}$-law (see Fig. 4 of Ref. [9]),

$$\tau_b = \frac{d^{0.3}}{C_2 e^{-E_b/RT} \cdot X_{\text{eff}}}, \tag{13}$$

where $C_2 = 8.72 \times 10^5$, $E_b = 73.6$ kJ/mol, d the particle diameter in μm, and R the universal gas constant. The burning time τ_b has a unit in second. It should be noted that agglomeration of small particles could occur in the experiments of Parr et al. [20]. The measured data might actually be the burning time of agglomerated particles with a larger size. More recently, Bazyn et al. [44] examined the combustion of aluminum particles in a well-controlled environment at a temperature of 2650 K and a pressure of 8 atm behind a reflected shock in a shock tube. Burning times were measured for two different particle diameters of 2.8 and 10.0 μm by observing the light emission of AlO. Results were globally correlated using a $d^{1.0}$-law. In the present work, both the $d^{0.3}$- and $d^{1.0}$-laws were examined, and the particle burning-time model was switched from the $d^{1.8}$-law to either the $d^{0.3}$- or the $d^{1.0}$-law at a particle size of around 12 μm.

As the particle gets even smaller, its diameter d becomes comparable to the mean free path, l, of the surrounding gas phase. The Knudsen number, defined as $Kn = 2 \cdot l/d$, is on the order of unity. Under such conditions, the continuum hypothesis for the gas-phase flowfield around an individual particle breaks down, and the $d^{1.0}$-model, based on the assumption that surface reactions prevail, may not be valid, since the transfer of heat and mass to/from the particle exhibits different characteristics. Further investigations by means of molecular-dynamics simulations are required to gain insight into the combustion mechanisms of ultra-fine particles.

4. Asymptotic behavior at molecular limit

The general analysis established in the preceding sections is valid for both nano- and micron-sized particles. As the particle shrinks to the sub-nano range, its behavior can be treated asymptotically as a big gaseous molecule. For example, the number of atoms in an aluminum particle decreases from 32×10^3 to 32 when the particle diameter decreases from 10 to 1 nm. The intermolecular bonding force in the bulk of a particle diminishes rapidly, as reflected by the melting temperature shown in Fig. 1. Two scenarios, passivated (preoxidized) and nascent (non-preoxidized) particles, are considered herein. The first case assumes that an oxide layer forms once the particle is exposed to air, as in the situation with finite-sized particles. The thickness of the oxide layer largely depends on the manufacturing process, and is normally on the order of several nanometers. Sanchez-Lopez et al. [45] studied the passivation of nano-sized aluminum particles prepared by the gas-phase condensation method. For particles in the range of 12–41 nm, an oxide layer with a 4 nm thickness is developed independent of oxygen dosage. A similar observation was made by Campell et al. [46] in their molecular-dynamics simulations of oxide-layer formation for a particle of 20 nm diameter under room conditions. Based on these experimental and computational results, particles in the sub-nanometer range are fully composed of inert oxide in a normal oxidizing environment. The associated flame speed of a particle dust in air goes to zero due to the lack of exothermic reactions.

Table 1
Al/O sub-mechanisms, $k = A \times T^n \exp(-E/RT)$.

No.	Reactions	A (cm^3/mol s)	n	E (cal/mol)
1	$Al + O_2 = AlO + O$	9.72E13	0.	159.95
2	$Al + O + M = AlO + M$	3.0E17	−1.0	0.
3	$AlO + O_2 = OAlO + O$	4.62E14	0.	19885.9
4	$Al_2O_3 = AlOAlO + O$	3.0E15	0.	97649.99
5	$Al_2O_3 = OAlO + AlO$	3.0E15	0.	126999.89
6	$AlOAlO = AlO + AlO$	1.0E15	0.	117900.
7	$AlOAlO = Al + OAlO$	1.0E15	0.	148900.
8	$AlOAlO = AlOAl + O$	1.0E15	0.	104249.94
9	$OAlO = AlO + O$	1.0E15	0.	88549.86
10	$AlOAl = AlO + Al$	1.0E15	0.	133199.94
11	$Al = Al(l)$	1.0E14	0.	0.
12	$Al_2O_3 = Al_2O_3(l)$	1.0E14	0.	0.

$k = A \times T^n \exp(-E/RT)$, provided by L. Catoire, University of Orleans, France, December 2004.

The second case deals with nascent particles by neglecting the presence of an oxide layer. Such a scenario exists if naked particles can instantly mix and react with the surrounding air in the flame region prior to the formation of any passivating layer on the particle surface. Under this condition, particles at sub-nano scales can be assumed to behave as large molecules. The associated particle-laden flow is modeled as a one-dimensional laminar, premixed system. The resultant flame speed represents the theoretical limit that an aluminum particle dust can possibly achieve in air. In the present study, the Al/O gas-phase kinetic mechanism of Catoire et al. [47–49], consisting of 8 species and 10 reactions, as listed in Table 1, is employed to simulate the chemical process. Thermochemistry data is adopted from the JANNAF table supplemented by Swihart and Catoire [50]. Transport properties are obtained either from Svehla [51] or calculated using molecular kinetics theory. The overall formulation is numerically solved with the CHEMKIN software package and the PREMIX subroutine [52].

In the model described above, ultra-fine nano-particles are assumed to be initially in the liquid state, a condition consistent with the low melting temperature of small particles, and then evaporate and react with the oxidizer in the gas phase. A partial equilibrium phase-transition process is presumed with a high rate constant. The hypothesis is further corroborated by chemical equilibrium calculations, indicating that replacing solid-phase aluminum with its liquid counterpart in the initial condition has very minor effects on the final combustion products and flame temperature. Thus only liquid and gaseous aluminum are considered to simplify the analysis. It is worth mentioning that the chemical kinetic mechanism listed in Table 1 includes gas-phase reactions of Al_2O_3. According to Ref. [53], Al_2O_3 does not exist in the gas phase, as aluminum oxide volatilizes exclusively by decomposi-

Author's personal copy

tion to gaseous sub-oxides and elements such as O_2, or by dissociation to species such as O. An equilibrium transition reaction was thus presumed for Al_2O_3. Finally, the transport properties of condensed-phase aluminum and alumina are taken to be those of their gas-phase counterparts. Obviously, with these assumptions, an idealized flame is constructed, and it may not exist in reality. The present analysis, however, does provide valuable information about the aluminum-aerosol flame in the sub-nanometer range. The work provides the maximum flame speed that can be achieved when the particle size is reduced to its molecular limit. Investigation of the effects of detailed chemical kinetics on the flame behavior in the molecular limit also sheds light on the processes of micron- and nano-sized aluminum particle combustion.

4.1. Chemical kinetics of aluminum/air reactions

The general behavior of the Al/O reaction was first examined using the SENKIN program [54], which numerically integrates the mass and energy conservation equations for a homogeneous mixture in a closed system. The purpose of the analysis is to identify the dominant chemical reaction pathways and heat-release mechanisms. In the following, the combustion of stoichiometric gaseous and liquid aluminum–air mixtures in an adiabatic, constant-pressure environment is investigated.

Fig. 3a shows the temperature evolution of a stoichiometric gaseous-aluminum/air mixture with five different initial temperatures of $T_0 = 300$, 1000, 2000, 2300, and 2800 K. In all the cases, reactions are completed on a time scale of ~0.1 μs with the final temperatures ranging from 3811 to 3964 K. The small difference in the maximum temperature may result from the vaporization–dissociation of the aluminum oxide [53]. For many metal–oxygen systems, the final flame temperature is usually limited by the vaporization–dissociation temperature of condensed oxides. This phenomenon may be attributed to the fact that the heat of vaporization–dissociation of the metal oxide exceeds the energy available for raising the temperature of the condensed-phase oxide above its 'boiling point.' Fig. 3b shows the evolution of species concentrations with $T_0 = 2300$ K. The final temperature is 3930 K. The dominant product species are O, AlO, AlOAl and Al_2O_3(l), with mole fractions of 0.150, 0.053, 0.031 and 0.028, respectively.

Calculations were also conducted for mixtures consisting of liquid aluminum and air. The phase change between liquid and gaseous aluminum is treated using a non-equilibrium analysis, as listed in Table 1. Fig. 4a shows the temperature evolution for four different initial temperatures of $T_0 = 1500$, 2000, 2300, and 2800 K. The ignition time decreases from 25 μs for $T_0 = 1500$ K to 0.5 μs for $T_0 = 2800$ K. The slight decrease in temperature during the early stage of each case results from the evaporation of liquid aluminum. The final equilibrium temperature ranges from 3742 to 3833 K. Fig. 4b shows the temporal evolution of species concentrations with $T_0 = 2300$ K. The final product temperature of 3803 K is lower than its gaseous counterpart by 127 K. The mole fraction of liquid Al_2O_3 in the products reaches 0.064, and the mole fraction of O reduces to 0.10.

Fig. 5 shows the dominant reaction pathways for a gaseous-aluminum/air system. The reactions proceed in a sequential, partially overlapping manner. The steps outlined herein are determined from analysis of reaction flux (defined as the net rate of forward and reverse reactions), which characterizes the dominant production and consumption mechanisms of reactant of interest. Two primary mechanisms for the direct consumption of gaseous aluminum are

$$Al + O_2 = AlO + O, \quad (R1)$$

$$AlOAl = AlO + Al. \quad (R10)$$

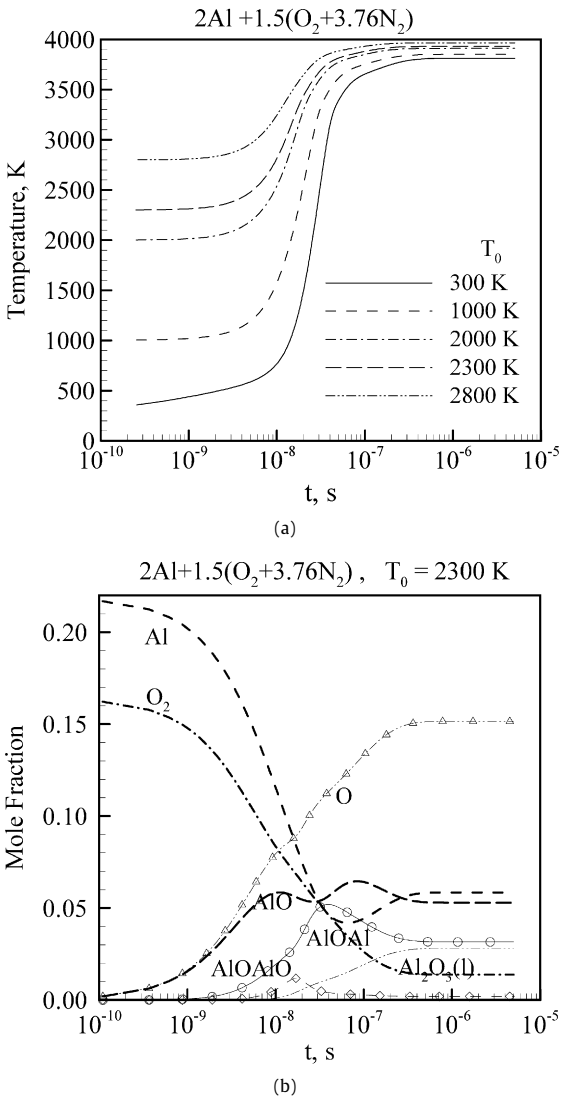

Fig. 3. Temporal evolution of temperature and species concentrations of a stoichiometric gaseous-aluminum/air mixture with various initial temperatures; particles treated asymptotically as molecules.

The dominant production mechanism of Al_2O_3 is

$$Al_2O_3 = AlOAlO + O. \quad (R4)$$

The reactions contributing to the formation of AlOAlO are

$$AlOAlO = AlO + AlO, \quad (R6)$$

$$AlOAlO = AlOAl + O. \quad (R8)$$

It can be observed that O atoms play an important role in the current reaction system. Oxygen atoms are required for the formation of Al_2O_3 and are also very active in the production of intermediate species AlOAlO. The production rates of these two species are directly related to the overall reaction rate. The primary reaction pathways for a liquid-aluminum/air mixture follow largely those of the gaseous-aluminum system described above and will not be discussed herein.

4.2. Flame characteristics of aluminum/air mixtures

Fig. 6 shows the calculated species-concentration and temperature distributions in a one-dimensional laminar flame of a stoichiometric mixture of liquid aluminum and air. The initial temperature T_0 is set to be 300 K. The flame propagates at a speed of

Author's personal copy

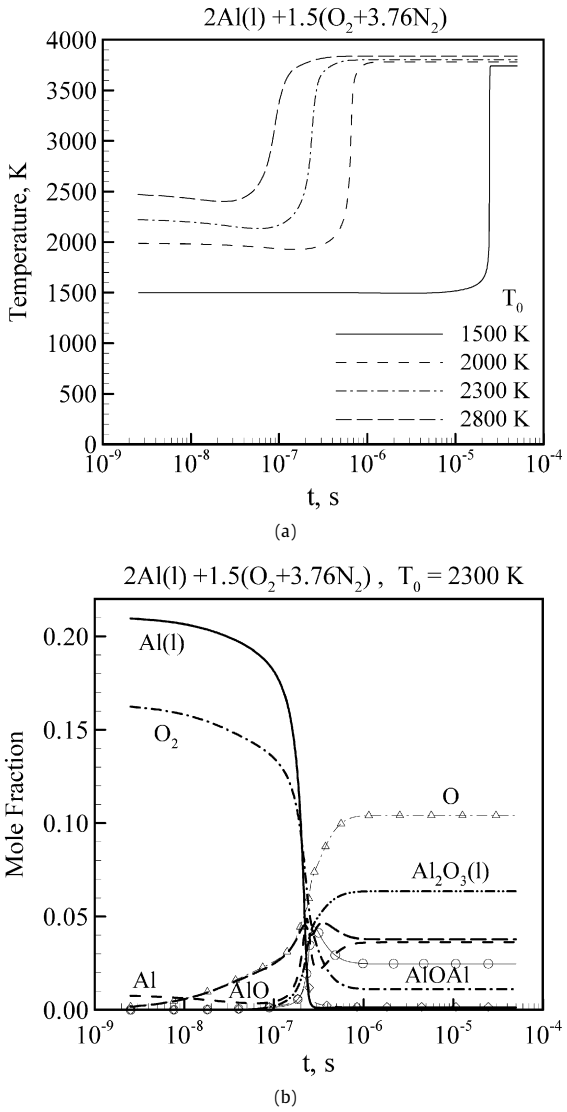

Fig. 4. Temporal evolution of temperature and species concentrations of a stoichiometric liquid-aluminum/air mixture with various initial temperatures; particles treated asymptotically as molecules.

Fig. 5. Dominant reaction pathways for gaseous-aluminum/air systems.

5.82 m/s, about 15 times of its counterpart for a methane/air mixture under the same conditions. The flame temperature is 3634 K, and the condensed phase Al_2O_3(l) is the main reaction product. For comparison, the burning velocity of a hydrogen/air mixture at the stoichiometric condition is 2.45 m/s. The corresponding flame temperature of 2364 K is over 1000 K lower than the value of an aluminum/air mixture.

Fig. 7 shows the adiabatic flame temperature and flame speed of a liquid-aluminum/air mixture as a function of the equivalence ratio. The mixture is preconditioned at a temperature of 300 K. For fuel-lean mixtures, both the adiabatic flame temperature and flame speed increase gradually with the equivalence ratio. A temperature plateau exists near the stoichiometric condition; this can be attributed to the limiting-temperature phenomenon caused by the evaporation and dissociation of condensed aluminum oxide Al_2O_3 [53].

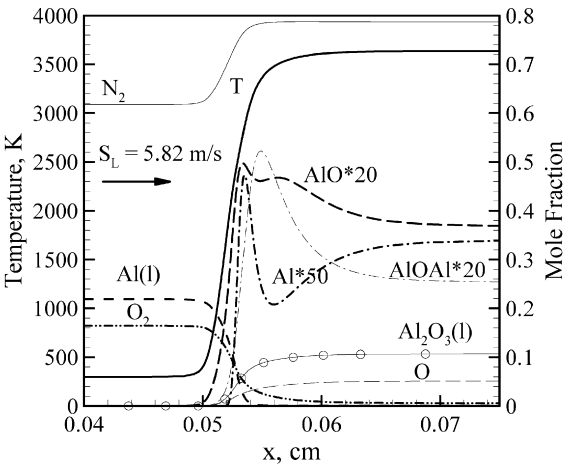

Fig. 6. Distribution of species concentrations and temperature in one-dimensional stoichiometric liquid-aluminum/air flame; particles treated asymptotically as molecules.

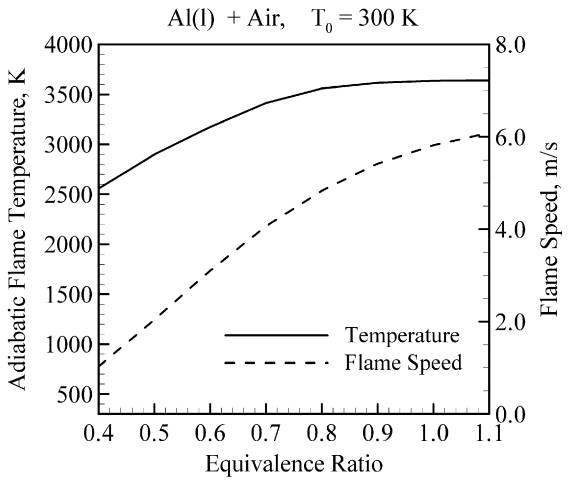

Fig. 7. Adiabatic flame temperature and flame speed in liquid-aluminum/air mixture as functions of equivalence ratio; particles treated asymptotically as molecules.

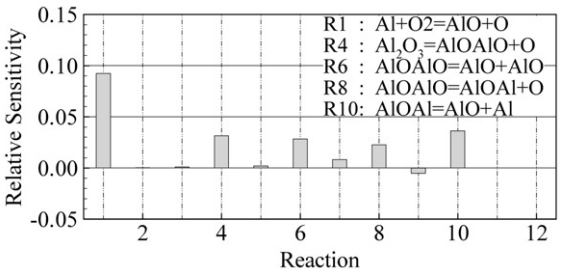

Fig. 8. Sensitivity of flame speed to reaction-rate constants for one-dimensional stoichiometric liquid-aluminum/air flame; particles treated asymptotically as molecules.

Fig. 8 shows the sensitivities of the flame speed to reaction-rate constants for a stoichiometric mixture of liquid aluminum and air. The most sensitive elementary reactions are the initiation reaction $Al + O_2 = AlO + O$ (R1), the Al_2O_3 formation reaction, $Al_2O_3 = AlOAlO + O$ (R4), and three intermediate reactions: $AlOAlO = AlO + AlO$ (R6), $AlOAlO = AlOAl + O$ (R8), and $AlOAl = AlO + Al$ (R10). Fig. 9 shows the sensitivities of the temperature field to reaction-rate constants. The most influential reaction, (R1), is identical to that found in the flame-speed sensitivity analysis shown in Fig. 8.

Author's personal copy

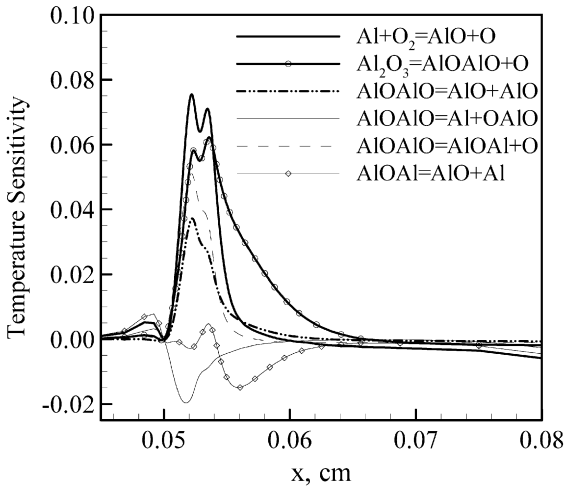

Fig. 9. Sensitivity of temperature field to reaction-rate constants for one-dimensional stoichiometric liquid-aluminum/air flame; particles treated asymptotically as molecules.

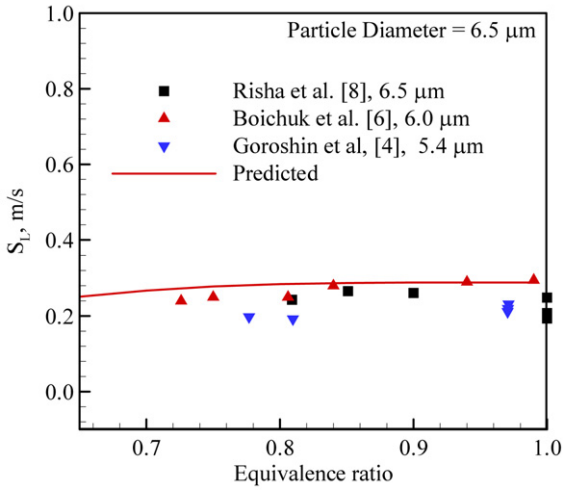

Fig. 10. Flame speed as a function of equivalence ratio in mixture of aluminum particle dust and air.

5. Combustion of aluminum particle dust in air

The overall analysis described above is employed to investigate the flame characteristics of fuel-lean mixtures of aluminum particles and air. A broad range of particle size at nano and micron scales is considered. Fig. 10 shows the predicted flame speed as a function of the equivalence ratio for a micron-sized particle dust/air mixture. The initial particle diameter is 6.5 μm, and the mixture is preconditioned at 300 K and 1 atm. The flame speed increases slightly with increasing particle concentration. Several sets of experimental data, from Goroshin et al. [4], Boichuk et al. [6], and Risha et al. [8], are plotted for comparison. Considerable scatter is observed in the experimental data due to the use of different experimental apparatuses. The predicted result falls in the upper range of measured values, around 0.2 m/s, mainly due to the neglect of heat losses to the ambient environment in the analysis. The predicted flame temperature is around 3500 K.

Fig. 11 shows the calculated flame speed as a function of particle diameter at a fuel-lean condition of $\phi = 0.85$. The solid lines represent the calculated flame speed, the black solid symbols the experimental data, the red filled circle the flame speed at the molecular limit, and the dashed lines the projected or conjectured

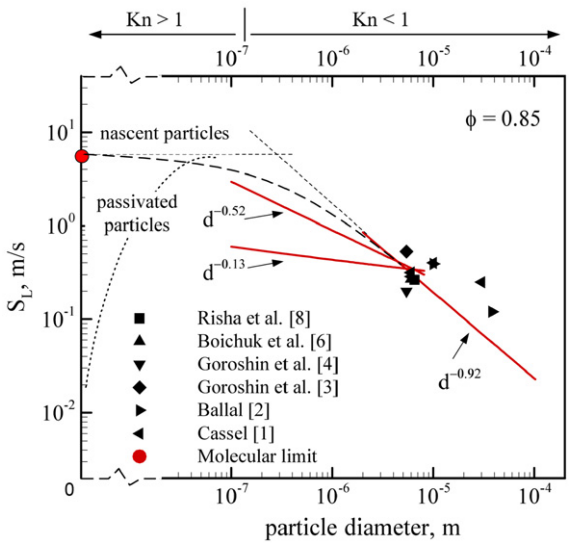

Fig. 11. Flame speed as a function of particle diameter in mixture of aluminum particle dust and air (solid lines: calculated flame speed; black solid symbols: experimental data; red filled circle: flame speed at molecular limit; dashed lines: projected or conjectured flame speed).

flame speed. The mixture is initially at room condition. Experimental data obtained from different measurements is also included. For micron-sized and larger particles, the flame speed increases with decreasing particle size, following a d^{-m}-law with m being 0.92. This value of m is about one half of the exponent n (= 1.8) in the particle-burning time model of Beckstead [43] for micron-sized particles given in Eq. (12). The theoretical predictions agree reasonably well with experimental results. As the particle size decreases to several micrometers, transition of the burning mechanism from a diffusion- to a kinetics-dominated mode occurs. A particle burning-time correlation which is different from Eq. (12) should thus be used. In the size range of 130 nm–10 μm, the flame speed follows the $d^{-0.52}$-law if a kinetically controlled $d^{1.0}$-law of the particle burning time is implemented in the flame model. When a $d^{0.3}$-law of the burning time, derived from the experimental data of Parr et al. [20], is used, the flame speed follows a $d^{-0.13}$-law. As the particle size is further reduced to around 130 nm, the Knudsen number reaches unity. The continuum hypothesis for the gas phase around the aluminum particle becomes invalid. A more advanced model is required to appropriately describe the combustion mechanism of particles. The maximum flame speed of 5.82 m/s is expected at the molecular limit of particles (i.e., $d \to 0$), as discussed in Section 4. Since $S_L \sim \sqrt{\alpha \cdot \dot{\omega}}$ for a premixed flame, chemical kinetics play a dominant role in determining the asymptotic value of the flame speed at the molecular limit when the particle size shrinks to the sub-nanometer range. The particle-size effect diminishes locally under this limiting condition. No universal law of flame speed exists for the entire range of particle sizes. The exponent in the flame-speed law varies between 0.0 and 0.92 in different size regimes.

The above analysis neglects the passivation effect of the particle oxidation layer and the resultant reduction of heat release in the size range of several nanometers or smaller. A different scenario exists for ultra-fine particles, for which the oxide layer occupies a significant fraction of the particle mass, corresponding to the case of preoxidated particles as described in Section 4. As the percentage of active aluminum and the energy content of the particle drop below a critical point, the flame speed of the particle-laden flow begins to decrease with decreasing particle size. In the extreme

Author's personal copy

situation, the energy release from particle oxidation may not even be able to sustain a flame.

In summary, as the particle size decreases, the flame speed of a particle dust/air mixture increases, and the combustion transits from a diffusion-controlled mode at micron scales to a kinetically controlled mode at nano scales. Without particle pre-oxidation, the flame speed may reach its theoretical limit of 5.82 ms if particles are treated as gaseous molecules in the sub-nanometer range.

6. Summary

A theoretical analysis has been established to study the combustion of aluminum particles in air in a well-characterized laminar particle-laden flow under fuel-lean conditions. Special attention is given to the effects of particle size at nano and micron scales on the burning behavior and flame structure. The flame is assumed to consist of a preheat zone and a heat-release zone. Solutions of the flame speed and temperature distribution are numerically obtained from the energy equation in the flame zone. Experimental data on the ignition temperatures and burning rates of nano- and micron-sized particles are incorporated into the analysis. In addition, the flame properties of ultra-fine particles in the sub-nanometer range are examined by treating asymptotically particles as large gaseous molecules. Calculated flame speeds agree reasonably well with experimental data. As the particle diameter decreases from the micron to the nano range, the flame speed increases and the combustion transits from a diffusion-controlled to a kinetically controlled mode.

It is well established that the flame speed of a laminar flow is proportional to the inverse of the square root of the chemical reaction time. For a particle-dust flame, the chemical reaction time can be characterized by the particle burning time, which is size dependent. The flame speed thus can be correlated with the particle diameter through a d-power law, as long as the particle burning time is expressed using the same law. For micron-sized and larger particles, the flame speed follows the $d^{-0.92}$-law. For nano-particles, the $d^{-0.52}$ dependence is obtained, if a $d^{1.0}$-law of burning time is implemented in the flame model. No universal law of flame speed is found to exist over the entire range of particle sizes at both nano and micron scales. The exponent in the flame-speed law varies between 0.0 and 0.92 in different particle-size regimes. Without particle preoxidation, the flame speed may reach its theoretical limit of 5.82 m/s when particles shrink to the sub-nano range. With particle preoxidation, as the percentage of active aluminum and the energy content of the particles shrink to below a critical point, the flame speed begins to decrease with decreasing particle size. In the extreme situation, the energy release from particle oxidation may not even be able to sustain a flame. Results of this kind provide valuable information about the combustion of a particle-laden flow in an energy-conversion system using particulate aluminum as a primary fuel.

Acknowledgments

This work was sponsored by the Office of Naval Research (ONR) under Grant No. N00014-03-1-0595. The support and encouragement provided by Dr. Gabriel Roy are gratefully acknowledged. The authors would like to thank Dr. Laurent Catoire for providing his latest version of the chemical kinetics model of Al/O gas phase reactions.

References

[1] H.M. Cassel, Reports of Investigations 6551, Bureau of Mines, 1963.
[2] D.R. Ballal, Proc. R. Soc. London A 385 (1983) 21–51.
[3] S. Goroshin, M. Bidabaid, J.H.S. Lee, Combust. Flame 105 (1996) 147–160.
[4] S. Goroshin, I. Fomenko, J.H.S. Lee, Proc. Combust. Inst. 26 (1996) 1961–1967.
[5] Y. Shoshin, E.L. Dreizin, AIAA J. 42 (7) (2004) 1416–1426.
[6] L.V. Boichuk, V.G. Shevchuk, A.I. Shvets, Combust. Explos. Shock Waves 38 (6) (2002) 651–654.
[7] S. Goroshin, M. Kolbe, J.H.S. Lee, Proc. Combust. Inst. 28 (2000) 2811–2817.
[8] G.A. Risha, Y. Huang, R.A. Yetter, V. Yang, Combust. Flame, submitted for publication.
[9] Y. Huang, G.A. Risha, V. Yang, R.A. Yetter, Proc. Combust. Inst. 31 (2007) 2001–2009.
[10] E.W. Price, R.K. Sigman, in: V. Yang, T.B. Brill, W.Z. Ren (Eds.), Solid Propellant Chemistry, Combustion and Motor Interior Ballistics, in: Progress in Astronautics and Aeronautics, vol. 185, AIAA, 2000, Chapter 2.18, pp. 663–687.
[11] V.A. Babuk, V.A. Vassiliev, V.V. Sviridov, in: V. Yang, T.B. Brill, W.Z. Ren (Eds.), Solid Propellant Chemistry, Combustion and Motor Interior Ballistics, in: Progress in Astronautics and Aeronautics, vol. 185, AIAA, 2000, Chapter 2.21, pp. 749–776.
[12] P. Bucher, L. Ernst, F.L. Dryer, R.A. Yetter, T.P. Parr, D.M. Hanson-Parr, in: V. Yang, T.B. Brill, W.Z. Ren (Eds.), Solid Propellant Chemistry, Combustion and Motor Interior Ballistics, in: Progress in Astronautics and Aeronautics, vol. 185, AIAA, 2000, Chapter 2.19, pp. 689–722.
[13] K.P. Brooks, M.W. Beckstead, J. Propul. Power 11 (4) (1995) 769–780.
[14] E.L. Dreizin, Combust. Flame 105 (1996) 541–556.
[15] P. Bucher, R.A. Yetter, F.L. Dryer, E.P. Vicenzi, T.P. Parr, D.M. Hanson-Parr, Combust. Flame 117 (1999) 351–361.
[16] P.E. DesJardin, J.D. Felske, M.D. Carrara, J. Propul. Power 21 (3) (2005) 478–485.
[17] A.P. Il'in, A.A. Gromov, V.I. Vereshchagin, E.M. Popenko, V.A. Surgin, H. Lehn, Combust. Explos. Shock Waves 37 (6) (2001) 664–668.
[18] Y.S. Kwon, A.A. Gromov, A.P. Ilyin, E.M. Popenko, G.H. Rim, Combust. Flame 133 (2003) 385–391.
[19] T.P. Parr, D. Hanson-Parr, R.A. Yetter, in: Proceedings of 36th JANNAF Combustion Subcommittee Meeting, October 1999.
[20] T.P. Parr, C. Johnson, D. Hanson-Parr, K. Higa, K. Wilson, in: 39th JANNAF Combustion Subcommittee Meeting, December 2003.
[21] J. Eckert, J.C. Holzer, C.C. Ahn, Z. Fu, W.L. Johnson, Nanostruct. Mater. 2 (1993) 407–413.
[22] S. Alavi, D.L. Thompson, J. Phys. Chem. A 110 (2006) 1518–1523.
[23] P. Puri, V. Yang, J. Phys. Chem. C 111 (2007) 11776–11783.
[24] C.R.M. Wronski, Br. J. Appl. Phys. 18 (1967) 1731–1737.
[25] R.A. Yetter, F.L. Dryer, Micro-Gravity Combustion: Fire in Free Fall, Academic Press, 2001, pp. 419–478.
[26] K. Park, D. Lee, A. Rai, D. Mukherjee, M.R. Zachariah, J. Phys. Chem. B 109 (2005) 7290–7299.
[27] M.A. Trunov, M. Schoenitz, F.L. Dreizin, Combust. Theory Modell. 10 (4) (2006) 604–623.
[28] T. Bazyn, H. Krier, N. Glumac, J. Propul. Power 21 (4) (2005) 577–582.
[29] H.H. Rosenbrock, Comput. J. 5 (1963) 329–330.
[30] W.H. Press, S.A. Teukolsky, W.T. Vetterling, B.P. Flannery, Numerical Recipes in Fortran 77: The Art of Scientific Computing, second ed., 1992.
[31] R. Fridman, A. Macek, Combust. Flame 6 (1962) 9–19.
[32] R. Fridman, A. Macek, Proc. Combust. Inst. 9 (1963) 703–709.
[33] A.G. Merzhanov, Yu.M. Grigorjev, Yu.A. Gal'chenko, Combust. Flame 29 (1977) 1–14.
[34] M.E. Derevyga, L.N. Stesik, E.A. Fedorin, Combust. Explos. Shock Waves 13 (1977) 722–726.
[35] V.A. Ermakov, A.A. Razdobreev, A.I. Skorik, V.V. Pozdeev, S.S. Smolyakov, Combust. Explos. Shock Waves 18 (1982) 256–257.
[36] C. Brossard, A. Ulas, C.L. Yen, K.K. Kuo, in: 16th International Colloquium on the Dynamic of Explosions and Reactive Systems, Krakow, Poland, 3–8 August 1997.
[37] S. Yuasa, Y. Zhu, S. Sogo, Combust. Flame 108 (1997) 387–396.
[38] C.J. Bulian, T.T. Kerr, J.A. Puszynski, in: 31st International Pyrotechnics Seminar, Fort Collins, CO, 12–14 July 2004, p. 327.
[39] Y. Zhu, Y. Yuasa, Combust. Flame 115 (1998) 327–334.
[40] I.G. Assovskiy, O.M. Zhigalina, G.P. Kuzhntsov, V.I. Kolesnikov-Svinarev, in: 5th International Microgravity Combustion Workshop, Cleveland, USA, May 18–20, 1999.
[41] M.A. Trunov, M. Schoenitz, F.L. Dreizin, Propell. Explos. Pyrotech. 30 (1) (2005) 36–42.
[42] A. Rai, D. Lee, K. Park, M.R. Zachariah, J. Phys. Chem. B 108 (2004) 14793–14795.
[43] M.W. Beckstead, Combust. Explos. Shock Waves 41 (5) (2005) 533–546.
[44] T. Bazyn, H. Krier, N. Glumac, Proc. Combust. Inst. 31 (2007) 2021–2028.
[45] J.C. Sanchez-Lopez, A.R. Gonzalez-Elipe, A. Fernandez, J. Mater. Res. 13 (3) (1998) 703–710.
[46] T. Campell, R.K. Kalia, A. Nakano, P. Vashishta, Phys. Rev. Lett. 82 (24) (1999) 4866–4869.
[47] L. Catoire, J.F. Legendre, M. Giraud, J. Propul. Power 19 (2) (2003) 196–202.

Author's personal copy

[48] M.T. Swihart, L. Catoire, B. Legrand, I. Gokalp, C. Paillard, Combust. Flame 132 (2003) 91–101.
[49] L. Catoire, private communication, December 2004.
[50] M.T. Swihart, L. Catoire, Combust. Flame 121 (2000) 210–222.
[51] R.A. Svehla, NASA Technical Report R-132, 1962.
[52] J.R. Kee, F.M. Rupley, J.A. Miller, Sandia National Laboratories Report SAND 89-8009B, Livermore, CA, 1992.
[53] I. Glassman, Combustion, third ed., Academic Press, 1996.
[54] A.E. Lutz, R.J. Kee, J.A. Miller, Sandia National Laboratories Report No. SAND87-8248, 1987.